Related F-box proteins control cell death in *Caenorhabditis elegans* and human lymphoma

Michael Chiorazzi[a,1], Lixin Rui[b,1,2], Yandan Yang[b], Michele Ceribelli[b], Nima Tishbi[a], Carine W. Maurer[a], Stella M. Ranuncolo[b], Hong Zhao[b], Weihong Xu[b], Wing-Chung C. Chan[c], Elaine S. Jaffe[d], Randy D. Gascoyne[e], Elias Campo[f], Andreas Rosenwald[g], German Ott[h], Jan Delabie[i], Lisa M. Rimsza[j,k], Shai Shaham[a,3], and Louis M. Staudt[b,3]

[a]Laboratory of Developmental Genetics, The Rockefeller University, New York, NY 10065; [b]Metabolism Branch, Center for Cancer Research, National Cancer Institute, Bethesda, MD 20892; [c]Departments of Pathology and Microbiology, University of Nebraska, Omaha, NE 68198; [d]Laboratory of Pathology, Center for Cancer Research, National Cancer Institute, Bethesda, MD 20892; [e]British Columbia Cancer Agency, Vancouver, BC, Canada V5Z 4E6; [f]Hospital Clinic, University of Barcelona, 08036 Barcelona, Spain; [g]Department of Pathology, University of Wurzburg, 97080 Wurzburg, Germany; [h]Department of Clinical Pathology, Robert-Bosch-Krankenhaus and Dr. Margarete Fischer-Bosch Institute for Clinical Pharmacology, 70376 Stuttgart, Germany; [i]Pathology Clinic, Oslo University Hospital, N-0424 Oslo, Norway; [j]Department of Pathology, University of Arizona, Tucson, AZ 85724; and [k]Southwest Oncology Group, Ann Arbor, MI 48106

Edited by Iva Greenwald, Columbia University, New York, NY, and approved January 24, 2013 (received for review October 4, 2012)

Cell death is a common metazoan cell fate, and its inactivation is central to human malignancy. In *Caenorhabditis elegans*, apoptotic cell death occurs via the activation of the caspase CED-3 following binding of the EGL-1/BH3-only protein to the antiapoptotic CED-9/BCL2 protein. Here we report a major alternative mechanism for caspase activation in vivo involving the F-box protein DRE-1. DRE-1 functions in parallel to EGL-1, requires CED-9 for activity, and binds to CED-9, suggesting that DRE-1 promotes apoptosis by inactivating CED-9. FBXO10, a human protein related to DRE-1, binds BCL2 and promotes its degradation, thereby initiating cell death. Moreover, some human diffuse large B-cell lymphomas have inactivating mutations in *FBXO10* or express *FBXO10* at low levels. Our results suggest that DRE-1/FBXO10 is a conserved regulator of apoptosis.

cancer | ubiquitin

Programmed cell death is a major cell fate that is required for proper development and homeostasis of multicellular organisms. Excess cell death is a hallmark of many human degenerative disorders (1–3), whereas evasion of cell death signals is a key requirement for tumor formation (4–6). Apoptotic cell death is mediated by activation of caspases, proteases whose role in cell death has been conserved in all metazoans examined (7–9). Although mutations in the caspase genes themselves are not frequently found in human malignancy samples, regulators of caspase activation are often mutated or dysregulated in human cancers (6, 10).

The nematode *Caenorhabditis elegans* has proved fertile ground for uncovering conserved regulators of apoptosis. In most *C. elegans* cells fated to die, the BH3-only domain protein EGL-1 binds to the BCL2-related protein CED-9, allowing for the release of CED-4 from CED-9. CED-4, a protein related to Apaf-1, then promotes activation of CED-3 caspase to induce cell death (11). A modified set of interactions governs apoptosis induction in mammalian cells (9). Although this canonical pathway operates in most *C. elegans* cells that die, a few cells are interesting exceptions, including the tail-spike cell. This cell is generated by fusion of two cells near the tail of the developing embryo. Following fusion, the binucleate cell extends a thin, microtubule-filled process toward the tip of the tail (12). Once a tail spike has formed, transcription of the *ced-3* caspase gene by the homeodomain protein PAL-1 promotes tail-spike cell death (10). Whereas the *ced-3* and *ced-4* genes are essential for tail-spike cell death, *egl-1* plays only a minor role (10). Thus, other genes are likely to substitute for *egl-1* to regulate caspase activation in this cell.

Here we show that DRE-1, a *C. elegans* F-box protein, is a major regulator of tail-spike cell death that functions in parallel to EGL-1. Furthermore, we demonstrate that a related human protein, FBXO10, can promote cell death and is functionally altered in diffuse large B-cell lymphomas. Our results support the notion that in both settings the F-Box proteins inhibit the activity of BCL2-related proteins.

Results

DRE-1 Promotes Tail-Spike Cell Death in *C. elegans*. To identify tail-spike cell death regulators, we mutagenized animals carrying a tail-spike cell promoter::GFP reporter transgene and searched for postembryonic larvae containing a surviving tail-spike cell. We identified seven independent mutants exhibiting a larval tail-spike cell (Table S1). One of these, *ns38*, displayed inappropriate cell survival elsewhere in the animal and failed to complement the *ced-3*(*n717*) mutation. The *ns39* mutation complemented known cell death mutations, was recessive (Table 1), had a strong tail-spike cell survival defect with 79% of animals possessing an inappropriately surviving cell (Table 1 and Table S1), and was further studied.

We mapped the *ns39* mutation to a 0.29 map-unit region on chromosome V. Three observations suggest that the gene *dre-1*, located in this region, is the gene affected in *ns39* mutants. First, sequencing of *dre-1* coding regions revealed a C-to-T point mutation at position 192 of exon 4 converting serine 275 to leucine (Fig. 1*F*). Second, larvae homozygous for either of two other *dre-1* alleles, *dh99* and *dh279* (13), also possessed a surviving tail-spike cell and these alleles failed to complement *ns39* (Fig. 1*F* and Table 1). Third, transgenic animals carrying ~30 kb of wild-type genomic DNA surrounding *dre-1* or a globally-expressed *dpy-30* promoter::*dre-1* cDNA (14) had fewer surviving tail-spike cells compared with *ns39* animals (Table S1 and Fig. S1 *E–G*).

The surviving tail-spike cell in *dre-1*(*ns39*) mutants is binucleate and extends a posteriorly directed process (Fig. 1*A*). To confirm that this cell is a bona fide tail-spike cell and not a different cell that inappropriately adopted features of tail-spike cell fate, we tested whether transcription of *ced-3* caspase in this cell depends on the gene *pal-1*, as has been previously shown for the tail-spike cell (10). Indeed, *ced-3* expression in *pal-1*(*ns114*); *dre-1*(*ns39*) double mutants was greatly reduced (Fig. S1 *A–D*). Furthermore, in *dre-1* mutants that were also homozygous for the *ced-5*(*n1812*) mutation, which blocks apoptotic corpse engulfment, a persistent cell corpse was absent in all animals with a surviving tail-spike

Author contributions: M. Chiorazzi, L.R., C.W.M., S.S., and L.M.S. designed research; M. Chiorazzi, L.R., Y.Y., N.T., and C.W.M. performed research; M. Chiorazzi, L.R., Y.Y., M. Ceribelli, C.W.M., S.M.R., H.Z., W.X., W.-C.C.C., E.S.J., R.D.G., E.C., A.R., G.O., J.D., and L.M.R. contributed new reagents/analytic tools; M. Chiorazzi, L.R., C.W.M., S.S., and L.M.S. analyzed data; and M. Chiorazzi, L.R., S.S., and L.M.S. wrote the paper.

The authors declare no conflict of interest.

This article is a PNAS Direct Submission.

[1]M. Chiorazzi and L.R. contributed equally to this work.

[2]Present address: Division of Hematology/Oncology, Department of Medicine, School of Medicine and Public Health, University of Wisconsin, Madison, WI 53705.

[3]To whom correspondence may be addressed. E-mail: shaham@rockefeller.edu or lstaudt@mail.nih.gov.

This article contains supporting information online at www.pnas.org/lookup/suppl/doi:10.1073/pnas.1217271110/-/DCSupplemental.

Table 1. *dre-1* is required for tail-spike cell death

Genotype	Tail-spike cell survival, %
Wild-type	0 ± 0
dre-1(*ns39*)	79 ± 3
dre-1(*dh99*)	12 ± 3
dre-1(*dh279*)	2 ± 1
dre-1(*ns39*)/+	0 ± 0
dre-1(*dh99*)/+	0 ± 0
dre-1(*ns39*)/*dre-1*(*dh99*)	25 ± 4
dre-1 synergizes with core apoptotic genes	
ced-3(*n2427*)	0 ± 0
ced-3(*n2427*); *dre-1*(*dh99*)	46 ± 4
ced-4(*n3158*)	74 ± 4
ced-4(*n3158*); *dre-1*(*dh99*)	91 ± 3
ced-9(*n1950*)	3 ± 3
ced-9(*n1950*); *dre-1*(*dh99*)	59 ± 4
ced-9 is required for *dre-1* function	
egl-1(*n1084n3082*)	30 ± 6
egl-1(*n1084n3082*) *dre-1*(*dh99*)	85 ± 4
egl-1(*n1084n3082*) *dre-1*(*ns39*)	94 ± 2
ced-9(*n2812*); *ced-3*(*n2427*)	0 ± 0
ced-3(*n2427*); *dre-1*(*ns39*)	98 ± 1
ced-9(*n2812*); *ced-3*(*n2427*); *dre-1*(*ns39*)	20 ± 4

Strains contain *nsIs25*; n >100; error: SEM.

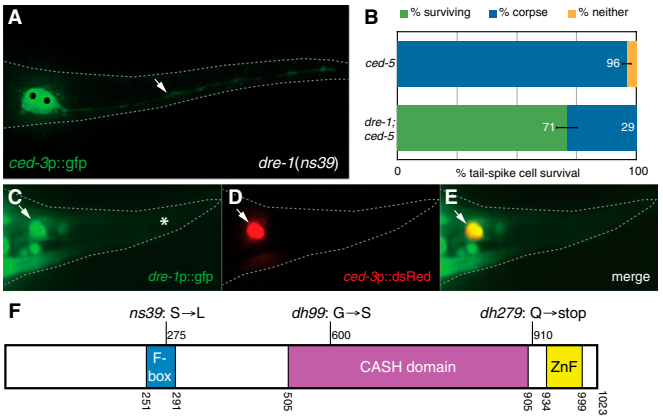

Fig. 1. *dre-1* promotes tail-spike cell death. (*A*) *dre-1*(*ns39*) L1 larva with a surviving tail-spike cell. Asterisks, tail-spike cell nuclei; dotted line, outline of the tail; arrow, tail-spike cell process. (*B*) Percentage of L1s with a surviving tail-spike cell (green), tail-spike cell corpse (blue), or neither (orange, a cell that has died and whose corpse has been cleared). The *ced-5*(*n1812*) and *dre-1*(*ns39*) alleles were used. Error bars, SEM. (*C–E*) *ced-3*(*n717*) larva expressing *dre-1*p::gfp (*C*), *ced-3*p::dsRed (*D*). (*E*) Merged image. Arrows, tail-spike cell nuclei. The asterisk denotes the region occupied by hyp10. Note the absence of GFP. (*F*) Schematic of DRE-1.

cell (Fig. 1*B*). Finally, animals homozygous for weak mutations in both *dre-1* and global cell death regulators (*ced-3*, *ced-4*, and *ced-9*) exhibited strong genetic interactions (Table 1), and, importantly, all double-mutant larvae exhibiting a tail-spike cell had only one such cell. *dre-1*(*ns39*) animals had no extra cells in the anterior pharynx, a region convenient for scoring the presence of inappropriately surviving cells (Table S1) (15, 16), suggesting that *dre-1* primarily regulates tail-spike cell death.

DRE-1 Is a Component of a Death-Promoting Skp–Cullin–F-box Complex in the Tail-Spike Cell. To determine in which cell *dre-1* functions, we examined the expression pattern of a *dre-1* promoter::GFP reporter transgene and found that it was robustly expressed in the tail-spike cell but not in the surrounding hyp10 hypodermal cell that forms the tail spike (Fig. 1 *C–E*). Consistent with a cell-autonomous function, *dre-1*(*ns39*) mutants carrying an *aff-1* promoter::*dre-1* cDNA, expressed specifically in the tail-spike cell (Fig. S2*E*), were strongly rescued for tail-spike cell survival (Table S1).

dre-1 is predicted to encode an F-box domain protein and was previously identified as a gene affecting developmental timing (13). However, neither animals carrying mutations in timing genes nor animals containing mutations in known DRE-1 interacting proteins (17) had tail-spike cell survival defects (Table S2). To test whether DRE-1 might act as part of an SCF (Skp–Cullin–F-box) ubiquitin E3 ligase complex to regulate tail-spike cell death, we examined animals subjected to RNAi against 20 Skp- and Cullin-related genes (Fig. S3). We found that *cul-1* RNAi, like *dre-1* or *ced-4* RNAi, produced a block in tail-spike cell death (Fig. 2*A*). *skr-1* RNAi gave a weak but significant effect ($P < 0.0016$) and animals homozygous for the weak *skr-1*(*sm151*) mutation also exhibited inappropriate tail-spike cell survival (Fig. 2*A*; $P < 0.000008$) (18). These observations raise the possibility that DRE-1, CUL-1, and SKR-1 function in an SCF complex to regulate cell death. To test this model, we cotransfected *Drosophila* S2 cells with myc::SKR-1 and either HA::DRE-1, HA::DRE-1(*ns39*), or HA::DRE-1(*dh99*) plasmids and immunoprecipitated lysates. Whereas wild-type HA::DRE-1 and HA::DRE-1(*dh99*) bound myc::SKR-1 efficiently (6.5- and 5.8-fold enrichment over background), HA::DRE-1(*ns39*) bound myc::SKR-1 less well (2.2-fold enrichment; Fig. 2*B*). Because the *ns39* lesion strongly affects tail-spike cell death and alters the F-box domain required for SCF complex formation (Fig. 1*F*), we conclude that an interaction between DRE-1 and SKR-1 is important in vivo for tail-spike cell death and that DRE-1 likely functions with SKR-1 and CUL-1 in an SCF complex in this context.

DRE-1 Functions in Parallel to *egl-1*/BH3-only and Requires *ced-9*/BCL2. Our genetic and physical interaction studies suggest that DRE-1 may function to inactivate a cell death inhibitor in the tail-spike cell. We therefore tested the possibility that DRE-1 substitutes for EGL-1 to inhibit CED-9 function. We found that *egl-1*(null) and *dre-1* mutations exhibited strong synergistic interactions (Table 1). Similarly, we found that RNAi against either *skr-1* or *ned-8* also enhanced tail-spike survival in *egl-1* mutants [42% and 53% survival, respectively (n = 100)]. Furthermore, whereas the tail-spike cell survived in nearly all *ced-3*(*n2427*); *dre-1*(*ns39*) double mutants, survival was greatly reduced in *ced-9*(lf); *ced-3*(*n2427*); *dre-1*(*ns39*) animals (Table 1). These results demonstrate that *dre-1* acts in parallel to *egl-1* and upstream of or in parallel to *ced-9*. To test whether DRE-1 and CED-9 could physically interact, we cotransfected *Drosophila* S2 cells with HA::DRE-1 and myc::CED-9 plasmids and immunoprecipitated lysates using anti-myc antibodies. We found that CED-9 weakly, but reproducibly, bound to DRE-1 (Fig. 2*C*), suggesting that direct binding of DRE-1 and CED-9 may be important. Nonetheless, we cannot rule out the possibility that additional targets of DRE-1 may be important for indirectly regulating CED-9 activity.

DRE-1–Related FBXO10 Regulates BCL2 Protein Levels. Because DRE-1 seems to act through the BCL2 homolog CED-9 to promote apoptosis in *C. elegans* and because BCL2 protein is often overexpressed in human B-cell lymphomas (reviewed in ref. 19), we wondered whether an F-box protein might control BCL2 function in lymphoma. Of the >35 human F-box proteins, only two resemble DRE-1 in containing a carbohydrate-binding proteins and sugar hydrolases (CASH) domain: FBXO10 and FBXO11. FBXO11 has been shown to control the levels of the BCL6 transcriptional regulator and is confined to the nucleus, making it unlikely to be a regulator of BCL2, which resides in the cytoplasm (20). A Flag epitope-tagged FBXO10 isoform was localized in the cytoplasm of transduced HEK293T cells (Fig. 3*A*), making FBXO10 a candidate regulator of BCL2, perhaps acting analogously to DRE-1.

To examine whether FBXO10 might regulate BCL2 protein levels, we measured steady-state BCL2 protein amounts by flow cytometry in lymphoma cell lines in which FBXO10 was ectopically expressed (Fig. 3*B*). Among ABC DLBCL (activated B-

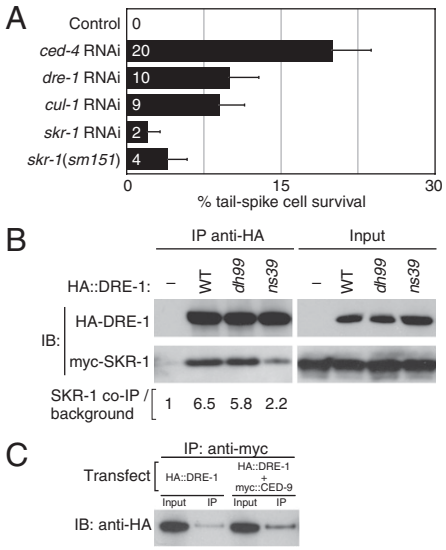

Fig. 2. DRE-1 acts in an SCF complex to promote death and binds CED-9. (*A*) Percentage of tail-spike cell survival in animals fed indicated RNAi constructs. All strains contain the *nsIs25* tail-spike cell reporter and the *rrf-3*(*pk1426*) RNAi-sensitizing mutation. Error bars, SEM. (*B*) S2 cells were transfected with myc::SKR-1 and the indicated HA::DRE-1 plasmid [none, –; wild type, WT; DRE-1(*dh99*) or DRE-1(*ns39*)]. Anti-HA beads were used for immunoprecipitation. Anti-myc or anti-HA antibodies were used for immunoblotting. (*C*) S2 cells were transfected with HA::DRE-1 alone or with myc::CED-9.

cell-like diffuse large B-cell lymphoma) lines, which have universally high BCL2 levels due to transcriptional up-regulation (Fig. S4), we observed a marked decrease in BCL2 abundance upon FBXO10 induction in three lines (OCI-Ly3, OCI-Ly10, and U2932). No change in BCL2 levels was observed in the ABC DLBCL line HBL1, which may be explained by our finding that HBL1 already has high FBXO10 expression (discussed below; Fig. 4*B*). BCL2 is also overexpressed in some GCB (germinal center B-cell-like) DLBCL cases due to a *t*(14, 18) translocation, and FBXO10 decreased BCL2 levels in cell-line models of this subtype (OCI-Ly19, Toledo) (Fig. 3*B*).

Because ectopic FBXO10 expression reduces steady-state BCL2 levels, we wondered whether knockdown of endogenous FBXO10 would increase steady-state BCL2 abundance. We identified three shRNAs whose expression reduced FBXO10 mRNA levels to varying degrees (Fig. 3*C*). Expression of these in HBL1 cells, which exhibit high levels of endogenous FBXO10 expression, increased BCL2 levels (Fig. 3*C*). By contrast, FBXO10 depletion had little, if any, effect on BCL2 levels in OCI-Ly3 cells, which have low endogenous FBXO10 expression (Figs. 3C and 4B). Thus, endogenous FBXO10 can control BCL2 levels.

To determine whether FBXO10 controls BCL2 protein stability, we measured BCL2 abundance over time after inhibition of new protein synthesis in HBL1 cells with cycloheximide. The half-life of BCL2, which was ~17 h in control shRNA-expressing cells, was much more prolonged (over 24 h) by FBXO10 depletion (Fig. 3*D*). By contrast, FBXO10 depletion had no effect on the half-life of the BCL2-related protein MCL1. Of note, there were no changes in BCL2 mRNA levels after knockdown of FBXO10. Together, these results suggest a direct role for FBXO10 in BCL2 protein stability.

To test this idea further, we investigated whether BCL2 may be a direct target of an FBXO10-containing ubiquitin ligase. To this end, we cotransfected 293T cells with vectors expressing Flag-tagged FBXO10 and HA-tagged BCL2 and observed robust coimmunoprecipitation of these proteins (Fig. 3*E*). As expected, the SKP1 and CUL1 proteins, subunits of all F-box-containing E3 ligases, were also present in the immune complexes containing FBXO10 and BCL2. To test for FBXO10-induced ubiquitination of BCL2, 293T cells were transduced with retroviral vectors expressing Flag-tagged FBXO10, MYC-tagged BCL2, and HA-tagged ubiquitin, and cells were treated with the proteasome inhibitor PS-341 to enhance the detection of ubiquitinated proteins. Following boiling and SDS lysis to disrupt noncovalent protein–protein interactions, the lysates were immunoprecipitated using an anti-MYC epitope antibody and analyzed by immunoblotting for HA-tagged ubiquitin (Fig. 3*F*). In the absence of FBXO10, a small amount of ubiquitinated BCL2 was detected as a smear of slow-migrating protein species, potentially due to the action of endogenous FBXO10 (or another ubiquitin ligase). In cells with ectopic FBXO10 expression, ubiquitinated BCL2 isoforms increased in abundance. In the lymphoma cell line HBL1, which has high levels of endogenous FBXO10 expression, an increase in ubiquitinated BCL2 was also observed after proteasome inhibition (Fig. S5). Together, these data suggest that FBXO10 is a component of a ubiquitin ligase that can target BCL2 protein for degradation.

FBXO10 Promotes Apoptosis in Lymphoma Cell Lines. Given the important antiapoptotic role of BCL2, we investigated FBXO10 expression and function in normal B-cell subpopulations and in human B-cell lymphomas. BCL2 expression varies considerably during normal B-cell differentiation, with germinal center B cells having the lowest levels, in part due to BCL-6–mediated repression of BCL2 mRNA expression (21, 22). In this regard, it was notable that FBXO10 mRNA levels were approximately fourfold higher in tonsillar germinal center B cells than in tonsillar naïve B cells (Fig. 4*A*). Although FBXO10 protein could not be examined due to lack of suitable antibodies, these data raised the possibility that FBXO10 might function in normal germinal center B cells and potentially in human B-cell lymphomas derived from these cells, such as diffuse large B-cell lymphoma (DLBCL) (19).

We therefore examined FBXO10 mRNA levels in primary DLBCL biopsy samples, including tumors belonging to the GCB and ABC subtypes. Despite the presumed derivation of GCB DLBCL tumors from germinal center B cells (23), many of these biopsies had relatively low FBXO10 mRNA levels (Fig. 4*A*), with one third (17/51) having levels that were below those of naïve B cells. ABC DLBCLs, which may derive from postgerminal center B cells, had similarly low FBXO10 mRNA expression in most cases, with 46% (24/52) having lower levels than naïve B cells (Fig. 4*A*). The mechanisms responsible for transcriptional down-regulation of FBXO10 in DLBCLs are unknown at present; no changes in FBXO10 promoter methylation were observed in cases with low expression.

We next sequenced the entire FBXO10 coding region in 154 lymphoma biopsy samples. FBXO10 sequence variants were detected in 5% (4/76) of GCB DLBCLs, including one frameshift and three missense mutations (H212N, V762L, and R825W) as well as in 1% (1/78) of ABC DLBCLs (R44H). No FBXO10 variants were detected in biopsy samples of primary mediastinal B-cell lymphoma ($n = 7$) or mantle-cell lymphoma ($n = 24$). All of the FBXO10 variants in DLBCL were heterozygous. One of these variants, H212N, has recently been identified as a rare SNP in the human population with a minor allele frequency of 1–1.4%, whereas the other variants have not been detected as SNPs in over 8,000 human samples (24, 25) and are presumed to be either somatic mutations or recent germ-line mutations. In this regard, it was notable that the SNP H212N was present in a GCB DLBCL case with the lowest FBXO10 expression, suggesting that it might not be functional (discussed below), whereas the V762L, R825W, and R44H mutants were in cases with higher FBXO10 mRNA expression (Fig. 4*A*). In summary, FBXO10 is frequently down-regulated transcriptionally in DLBCL compared with normal B cells and can be targeted by mutations.

The low expression of FBXO10 and the potentially deleterious FBXO10 mutations in some DLBCL tumors suggested that FBXO10 might function to promote cell death as does DRE-1 in *C. elegans*. To test this, we used a panel of human lymphoma lines that have a range of FBXO10 mRNA levels (Fig. 4*B*). We engineered these lines to enable doxycycline-inducible expression of FBXO10 together with GFP using retroviral vectors.

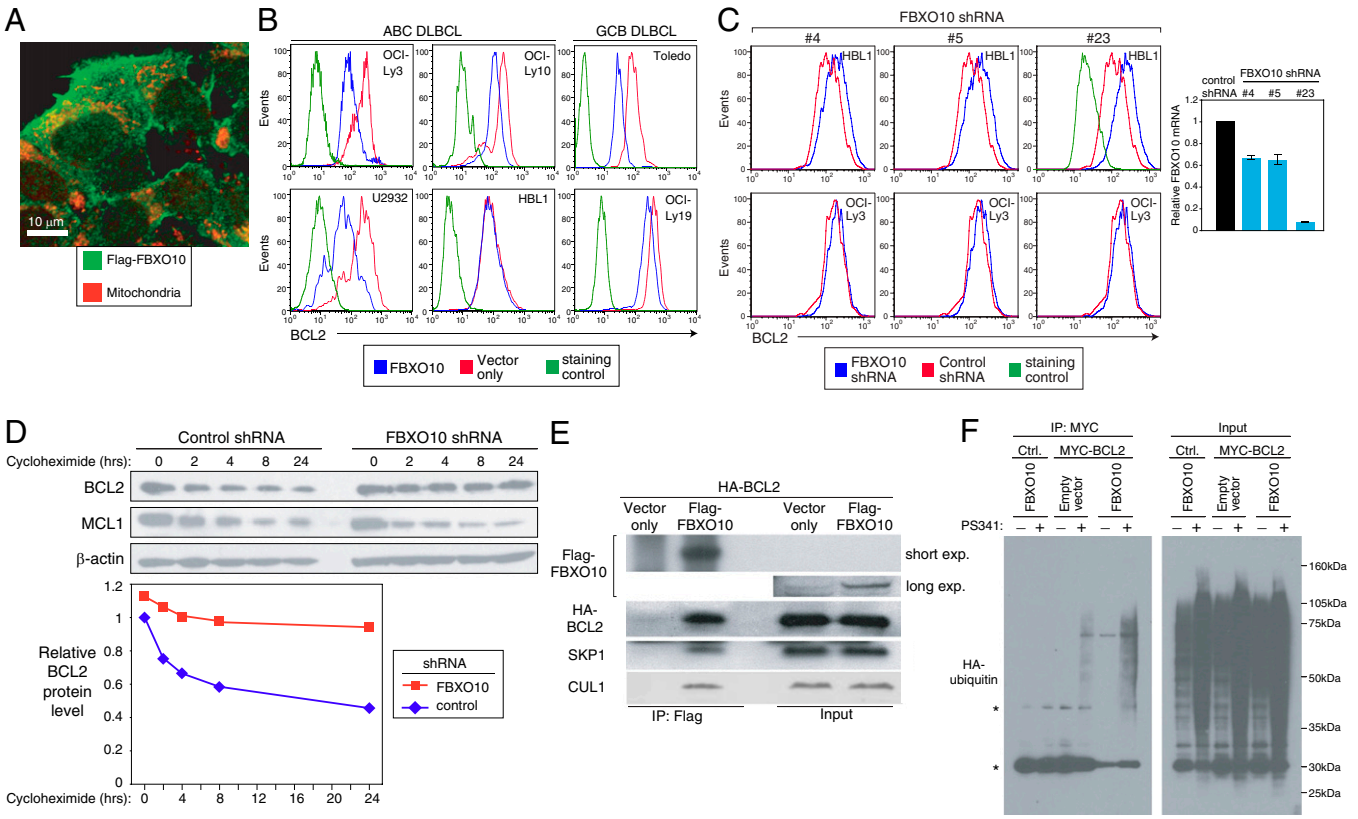

Fig. 3. FBXO10 regulates BCL2 protein stability. (*A*) 293T cells expressing Flag epitope-tagged FBXO10. (*B*) Ectopic FBXO10 decreases BCL2 expression in lymphoma lines. BCL2 levels, intracellular flow cytometry (IFC). (*C*) HBL1 cells (high FBXO10) and OCI-Ly3 cells (low FBXO10) expressing shRNAs targeting FBXO10. (*Right*) Degree of knockdown (quantitative PCR). (*D*) FBXO10 destabilizes BCL2. HBL1 cells were treated with cycloheximide, analyzed by immunoblotting and densitometry. (*E*) Co-IP of FBXO10 and BCL2. (*F*) FBXO10 promotes BCL2 ubiquitination in 293T cells. Ctrl, irrelevant MYC-tagged protein; PS-341, proteasome inhibitor. Asterisks denote nonspecific bands.

Following FBXO10 induction, we monitored viable FBXO10-expressing (GFP+) cells over time by flow cytometry. In a time-dependent fashion, FBXO10 expression affected the viability of more than half of the cell lines tested: 5/6 ABC DLBCL, 4/8 GCB DLBCL, 4/6 MCL (mantle cell lymphoma) cell lines, and 1/3:00 PMBL (primary mediastinal B-cell lymphoma) cell lines (Fig. 4*C*). That FBXO10 expression did not induce cell death in all lines makes it unlikely that the protein is generically cytotoxic. FBXO10 toxicity was roughly related to the level of endogenous FBXO10 mRNA: Within each lymphoma subtype, the lines with the highest FBXO10 expression were insensitive to ectopic FBXO10 expression whereas those with the lowest FBXO10 expression were sensitive (Fig. 4 *B* and *C*). The FBXO10-induced toxicity in these assays could be due to either increased apoptosis or decreased cell proliferation. Flow cytometric analysis of activated caspase-3 and cleaved polyADP ribose polymerase (PARP) indicated that FBXO10 expression induced apoptosis of both OCI-Ly3 and Rec-1 cells (Fig. 4*D*). Analysis of the cell cycle by flow cytometry revealed that FBXO10 expression did not inhibit cell proliferation (Fig. 4*E*), consistent with a role in modulating apoptosis in lymphoma cells.

We next wondered whether ectopic BCL2 expression could rescue the cell death induced by FBXO10 expression. For two FBXO10-sensitive lymphoma lines (U2932 and Rec-1), we generated stable clones with ectopic BCL2 expression by retroviral transduction and created control clones using an empty retroviral vector. The BCL2-expressing clones had 1.6- to 1.7-fold higher BCL2 expression than the control clones (Fig. 4*F*). We transduced these clones with retroviruses expressing FBXO10 plus GFP or GFP alone and tracked viable GFP+ cells over time following induction of FBXO10 expression. In the BCL2-expressing clones, more than 50% of the FBXO10+ cells remained viable at 3 d compared with less than 30% viability in the control clones (Fig. 4*F*). Thus, BCL2 can partially rescue lymphoma cells from FBXO10-induced death, consistent with its role as a negative regulator of BCL2 protein stability.

Functional Analysis of FBXO10 Mutations. The FBXO10 missense mutations in DLBCL occur at evolutionarily conserved residues, suggesting that they might be deleterious (Fig. 5*A*). R44H is localized to the F-box domain and thus might perturb ubiquitin ligase function. The V762L and R825W are located in CASH domains, which are putatively involved in substrate binding. To evaluate the effects of these mutations on FBXO10 function, we inducibly expressed FBXO10 mutants, or wild-type FBXO10, in OCI-Ly3 cells, because this line has very low levels of endogenous FBXO10 and dies readily when FBXO10 is ectopically expressed. As above, we tracked GFP+ transduced cells over time and observed that the V762L, R825W, and R44H FBXO10 mutants were less toxic than wild-type FBXO10 (Fig. 5*B*), indicating loss of function. As a control, we expressed an FBXO10 isoform lacking the F-box (ΔF-box), which presumably cripples the protein's ability to form a ubiquitin ligase. The ΔF-box isoform was not as toxic as wild-type FBXO10 but still retained some activity, possibly because this mutant can still bind to BCL2 (discussed below). Because the FBXO10 mutants from human DLBCL tumors were roughly as toxic as ΔF-box, we surmise that they are significantly impaired in function.

Because the R44H mutation alters the F-box, we wondered whether the mutant protein would form the predicted SCF E3 ubiquitin ligase complex. In coimmunoprecipitation experiments in 293T cells, FBXO10 R44H was unable to bind the SCF subunit SKP1, like the ΔF-box isoform (Fig. 5*C*), demonstrating that the diminished activity of the R44H mutants is due to their inability

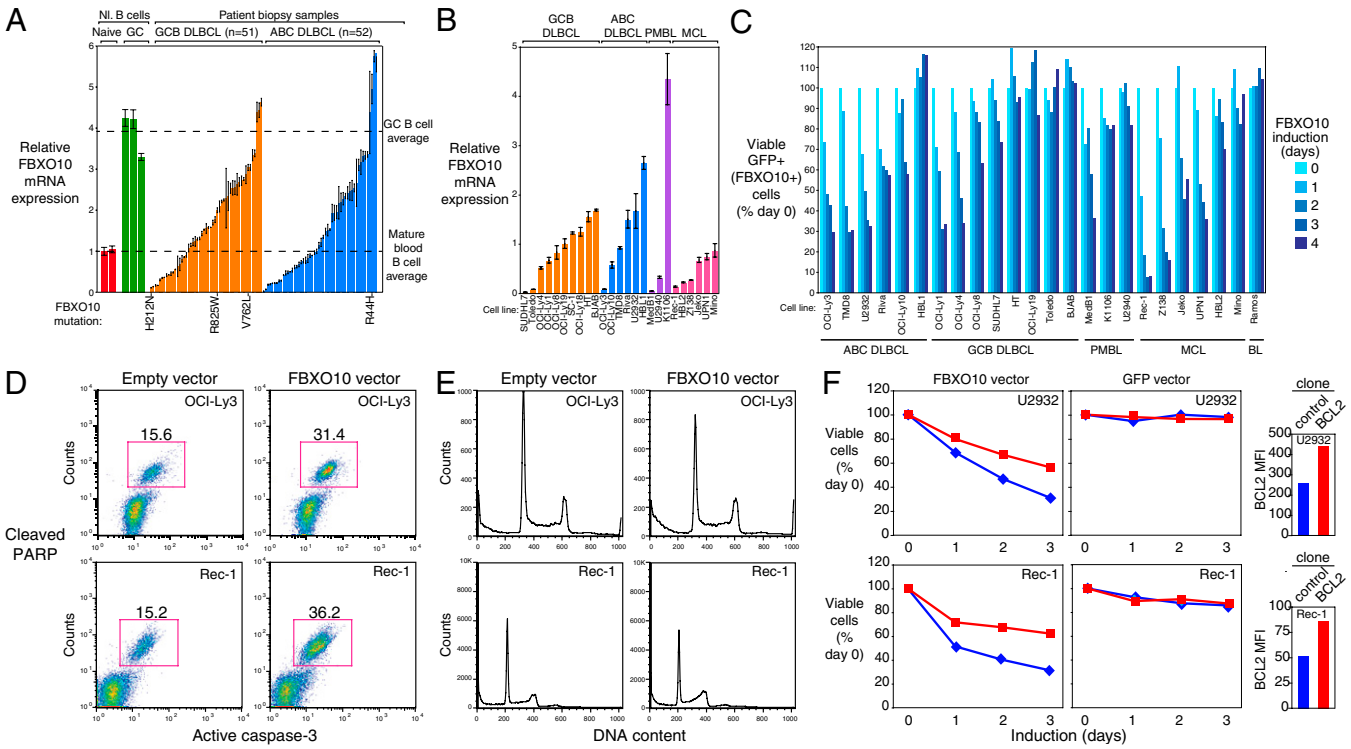

Fig. 4. FBXO10 promotes apoptosis in lymphomas. Quantitative PCR of FBXO10 mRNA in tumors (*A*) and cell lines (*B*). Error bars, SD ($n = 3$). (*C*) FBXO10 toxicity in lymphoma cell lines. Lines were transduced with FBXO10 and GFP. Viable GFP+ cells were counted after FBXO10 induction. More than 5,000 viable cells were examined. (*D*) Percentage of apoptotic cells with activated caspase-3 and cleaved PARP following FBXO10 transduction. (*E*) Cells from *D* stained with propidium iodide for DNA content. (*F*) Ectopic BCL2 rescues FBXO10-induced toxicity. Clones overexpressing BCL2 are compared with empty vector control [mean fluorescence intensity (MFI), *Right*]. Percentage of viable cells following doxycycline induction of FBXO10 as in *C*. Negative control, GFP only.

to participate in an SCF ubiquitin ligase complex. In contrast, the V762L or R825W mutants were not impaired in their interaction with SKP1. The ΔF-box isoform retained full ability to coimmunoprecipitate with BCL2, demonstrating that the region of FBXO10 C-terminal to the F-box is responsible for BCL2 recognition. Although FBXO10 V762L and R825W mutants were not impaired in their ability to bind BCL2, neither reduced BCL2 protein levels to the same extent as the wild-type FBXO10, consistent with a partial loss of function (Fig. 5*D*). That three FBXO10 missense mutants are impaired in their ability to destabilize BCL2 and kill lymphoma cells provides a rationale for their genetic selection in human lymphoma. Future investigations

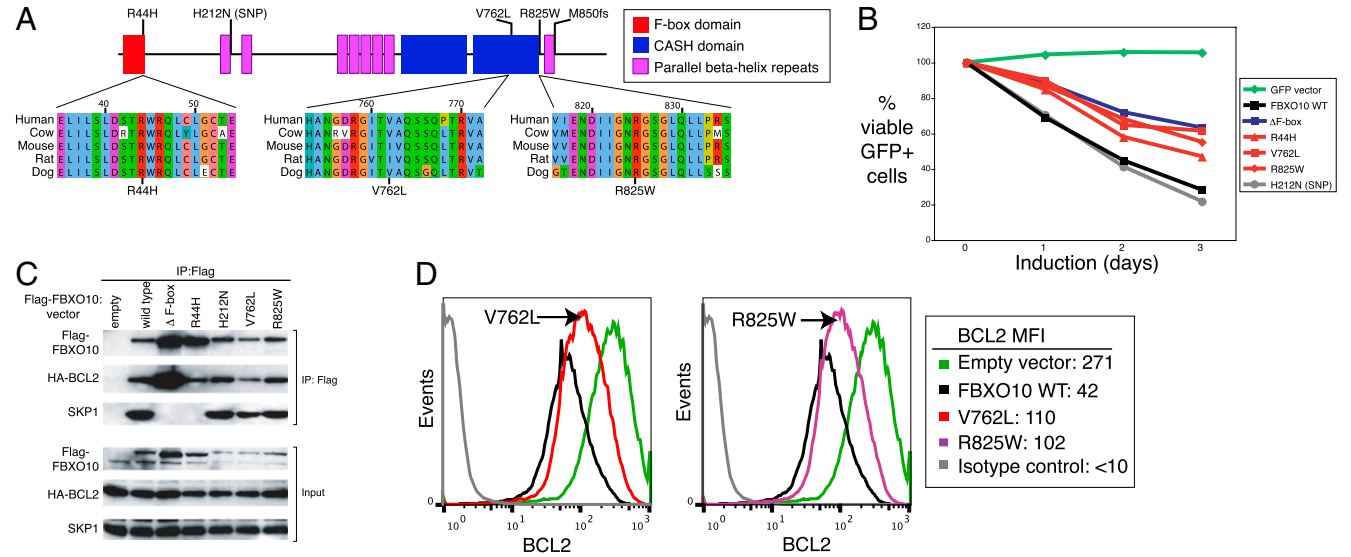

Fig. 5. FBXO10 mutants from human lymphomas. (*A*) Location and conservation of FBXO10 DLBCL mutations. fs, frameshift. (*B*) Toxicity of FBXO10 mutants in OCI-Ly3 cells (Refer to Fig. 3*C*; $n = 3$). (*C*) Effect of FBXO10 mutations on FBXO10 protein–protein interactions in 293T cells. (*D*) FBXO10 cancer mutations attenuate decrease in BCL2. Cell line, U2932. Histograms and mean fluorescence intensity (MFI) of BCL2 are shown.

DEVELOPMENTAL BIOLOGY

into the structural basis of FBXO10 action will be needed to fully understand why the V762L and R825W mutants are impaired in function.

Discussion

Protein degradation has been implicated in regulating BCL2-family members, including Bim, Bid, and MCL-1 (26–29). BCL2 has also been reported to be degraded by the proteasome (30–33); however, the functional and physiological consequences of this have not been extensively explored. This study brings together genetic and functional data from *C. elegans* and human cancer to demonstrate that DRE-1 and a related human protein, FBXO10, control apoptosis, and presents several lines of evidence supporting the notion that DRE-1 and FBXO10 control the stability of the antiapoptotic proteins CED-9 and BCL2, respectively, in vivo. Whereas BCL2 transcription in lymphoma can be promoted by chromosomal translocation, genome copy number alteration and epigenetic regulation, mechanisms that promote BCL2 protein stabilization in this context are less understood. FBXO10 could provide a foothold into a pathway that regulates the turnover of BCL2 protein in lymphoma cells and possibly also in normal B cells.

Down-regulation of FBXO10 mRNA expression is one mechanism by which FBXO10 activity may be attenuated in human lymphomas. Germinal center B cells, the normal cellular counterpart of GCB DLBCL, have virtually no expression of BCL2 protein despite expressing BCL2 mRNA (34). FBXO10 mRNA levels were roughly fourfold higher in germinal center B cells than in resting blood B cells, suggesting that FBXO10 could contribute posttranslationally to the low BCL2 protein levels in germinal center B cells. The majority of GCB DLBCL tumors had lower FBXO10 mRNA levels than normal germinal center B cells, and over a third had lower levels than resting blood B cells, consistent with a tumor suppressor mechanism. A second, less common, mechanism to impair FBXO10 function in lymphomas is the acquisition of missense FBXO10 mutations that reduce its ability to down-regulate BCL2 and its toxicity for these lymphoma cells. Interestingly, the FBXO10 mutations we identified in lymphoma were all heterozygous and seemed to be hypomorphic, but not null, alleles. This suggests that a full loss of FBXO10 function is not compatible with the development of lymphoma, and that FBXO10 functions as a haploinsufficient tumor suppressor. Intriguingly, complete loss of *dre-1* function in *C. elegans* produces embryonic inviability, suggesting the possibility of a critical cellular role in *C. elegans* as well. These observations suggest that both FBXO10 and DRE-1 likely regulate the abundance of other protein targets besides BCL2 and CED-9, respectively.

Our studies also highlight a previously undescribed mechanism of cell death regulation in *C. elegans*. Although cell death in this organism is mainly thought to be controlled by lineage-dependent transcription of the *egl-1* BH3-domain gene, our results demonstrate an important role for DRE-1, acting in lieu of EGL-1. Given the broad similarities in cell death regulation between *C. elegans* and mammals, we suggest that future identification in *C. elegans* of genes involved in DRE-1 function may reveal novel regulators of mammalian tumorigenesis and developmental cell death.

Materials and Methods

Standard methods were used to culture *C. elegans*. Ubiquitination assays were performed in the presence of proteasome inhibitors. See details in *SI Materials and Methods*.

ACKNOWLEDGMENTS. We thank members of the S.S. and L.M.S. laboratories for comments and the Shohei Mitani for strain *C05C8.6*(*tm3719*). Some nematode strains used were provided by the *Caenorhabditis* Genetics Center. This work was supported by National Research Service Award F30AG035484 from the National Institutes of Health (NIH)/National Institute on Aging (NIA) (to M. Chiorazzi); NIH Medical Scientist Training Program Grant GM07739 (to M. Chiorazzi); a C. J. Martin Fellowship from the National Health and Medical Research Council of Australia (to L.R.); NIH Grants R01HD042680 and R01NS081490 (to S.S.); National Cancer Institute (NCI) Strategic Partnerships to Evaluate Cancer Signatures Grant UO1-CA 114778; and the Intramural Research Program of the NIH, NCI, Center for Cancer Research.

1. Dawson TM, Ko HS, Dawson VL (2010) Genetic animal models of Parkinson's disease. *Neuron* 66(5):646–661.
2. Heintz N, Zoghbi HY (2000) Insights from mouse models into the molecular basis of neurodegeneration. *Annu Rev Physiol* 62:779–802.
3. Davies SW, et al. (1997) Formation of neuronal intranuclear inclusions underlies the neurological dysfunction in mice transgenic for the HD mutation. *Cell* 90(3):537–548.
4. Hanahan D, Weinberg RA (2000) The hallmarks of cancer. *Cell* 100(1):57–70.
5. Strasser A, Harris AW, Cory S (1991) bcl-2 transgene inhibits T cell death and perturbs thymic self-censorship. *Cell* 67(5):889–899.
6. Vaux DL, Cory S, Adams JM (1988) Bcl-2 gene promotes haemopoietic cell survival and cooperates with c-myc to immortalize pre-B cells. *Nature* 335(6189):440–442.
7. Yuan J, Shaham S, Ledoux S, Ellis HM, Horvitz HR (1993) The C. elegans cell death gene ced-3 encodes a protein similar to mammalian interleukin-1 beta-converting enzyme. *Cell* 75(4):641–652.
8. Liu X, Kim CN, Yang J, Jemmerson R, Wang X (1996) Induction of apoptotic program in cell-free extracts: Requirement for dATP and cytochrome c. *Cell* 86(1):147–157.
9. Abraham MC, Shaham S (2004) Death without caspases, caspases without death. *Trends Cell Biol* 14(4):184–193.
10. Maurer CW, Chiorazzi M, Shaham S (2007) Timing of the onset of a developmental cell death is controlled by transcriptional induction of the C. elegans ced-3 caspase-encoding gene. *Development* 134(7):1357–1368.
11. Conradt B (2009) Genetic control of programmed cell death during animal development. *Annu Rev Genet* 43:493–523.
12. Sulston JE, Schierenberg E, White JG, Thomson JN (1983) The embryonic cell lineage of the nematode Caenorhabditis elegans. *Dev Biol* 100(1):64–119.
13. Fielenbach N, et al. (2007) DRE-1: An evolutionarily conserved F box protein that regulates C. elegans developmental age. *Dev Cell* 12(3):443–455.
14. Hsu DR, Chuang PT, Meyer BJ (1995) DPY-30, a nuclear protein essential early in embryogenesis for Caenorhabditis elegans dosage compensation. *Development* 121(10):3323–3334.
15. Ellis RE, Horvitz HR (1991) Two C. elegans genes control the programmed deaths of specific cells in the pharynx. *Development* 112(2):591–603.
16. Ellis RE, Jacobson DM, Horvitz HR (1991) Genes required for the engulfment of cell corpses during programmed cell death in Caenorhabditis elegans. *Genetics* 129(1):79–94.
17. Li S, et al. (2004) A map of the interactome network of the metazoan C. elegans. *Science* 303(5657):540–543.
18. Killian DJ, et al. (2008) SKR-1, a homolog of Skp1 and a member of the SCF(SEL-10) complex, regulates sex-determination and LIN-12/Notch signaling in C. elegans. *Dev Biol* 322(2):322–331.
19. Shaffer AL, 3rd, Young RM, Staudt LM (2012) Pathogenesis of human B cell lymphomas. *Annu Rev Immunol* 30:565–610.
20. Duan S, et al. (2012) FBXO11 targets BCL6 for degradation and is inactivated in diffuse large B-cell lymphomas. *Nature* 481(7379):90–93.
21. Ci W, et al. (2009) The BCL6 transcriptional program features repression of multiple oncogenes in primary B cells and is deregulated in DLBCL. *Blood* 113(22):5536–5548.
22. Saito M, et al. (2009) BCL6 suppression of BCL2 via Miz1 and its disruption in diffuse large B cell lymphoma. *Proc Natl Acad Sci USA* 106(27):11294–11299.
23. Alizadeh AA, et al. (2000) Distinct types of diffuse large B-cell lymphoma identified by gene expression profiling. *Nature* 403(6769):503–511.
24. Abecasis GR, et al.; 1000 Genomes Project Consortium (2010) A map of human genome variation from population-scale sequencing. *Nature* 467(7319):1061–1073.
25. Tennessen JA, et al.; Broad GO; Seattle GO; NHLBI Exome Sequencing Project (2012) Evolution and functional impact of rare coding variation from deep sequencing of human exomes. *Science* 337(6090):64–69.
26. Akiyama T, et al. (2003) Regulation of osteoclast apoptosis by ubiquitylation of proapoptotic BH3-only Bcl-2 family member Bim. *EMBO J* 22(24):6653–6664.
27. Ley R, Balmanno K, Hadfield K, Weston C, Cook SJ (2003) Activation of the ERK1/2 signaling pathway promotes phosphorylation and proteasome-dependent degradation of the BH3-only protein, Bim. *J Biol Chem* 278(21):18811–18816.
28. Tait SW, et al. (2007) Apoptosis induction by Bid requires unconventional ubiquitination and degradation of its N-terminal fragment. *J Cell Biol* 179(7):1453–1466.
29. Zhong Q, Gao W, Du F, Wang X (2005) Mule/ARF-BP1, a BH3-only E3 ubiquitin ligase, catalyzes the polyubiquitination of Mcl-1 and regulates apoptosis. *Cell* 121(7):1085–1095.
30. Basu A, Haldar S (2002) Signal-induced site specific phosphorylation targets Bcl2 to the proteasome pathway. *Int J Oncol* 21(3):597–601.
31. Breitschopf K, Haendeler J, Malchow P, Zeiher AM, Dimmeler S (2000) Post-translational modification of Bcl-2 facilitates its proteasome-dependent degradation: Molecular characterization of the involved signaling pathway. *Mol Cell Biol* 20(5):1886–1896.
32. Dimmeler S, Breitschopf K, Haendeler J, Zeiher AM (1999) Dephosphorylation targets Bcl-2 for ubiquitin-dependent degradation: A link between the apoptosome and the proteasome pathway. *J Exp Med* 189(11):1815–1822.
33. Lin SS, et al. (2006) PP2A regulates BCL-2 phosphorylation and proteasome-mediated degradation at the endoplasmic reticulum. *J Biol Chem* 281(32):23003–23012.
34. Chleq-Deschamps CM, et al. (1993) Topographical dissociation of BCL-2 messenger RNA and protein expression in human lymphoid tissues. *Blood* 81(2):293–298.

Supporting Information

Chiorazzi et al. 10.1073/pnas.1217271110

SI Materials and Methods

Strains. All strains were maintained at 20 °C on nematode growth medium (NGM) agar with OP50 bacteria as previously described (1). The wild-type strain was N2 Bristol. The following strains were used:

LGI: *lin-28(n719), skr-1(sm151)*;

LGII: *aff-1(tm2214), lin-29(n333), lin-4(e912), rrf-3(pk1426)*;

LGIII: *ced-4(n3158), ced-9(n2812, n1950), pal-1(ns114)*;

LGIV: *ced-3(n717, n2427, n2436, ns38), ced-5(n1812)*;

LGV: *dre-1(ns39, dh99, dh279,), egl-1(n1084n3082), lin-46 (ma164), C05C8.6(tm3719)*; and

LGX: *nsIs25* (*ced-3*p::gfp+pRF4).
nsEx3098 (WRM067bH07 + *unc-122*p::dsRed); *dre-1*(*ns39*); *nsIs25*

nsEx3099 (WRM0637aG11 + *unc-122*p::dsRed); *dre-1*(*ns39*); *nsIs25*

*nsEx3102 (aff-1*p::*dre-1* cDNA + *unc-122*p::dsRed); *dre-1 (ns39); nsIs25*

*nsEx3103 (dpy-30*p::*dre-1* cDNA + *unc-122*p::dsRed*)*; *dre-1 (ns39); nsIs25*

*nsEx3106 (aff-1*p::*dre-1*(Y740C) cDNA + *unc-122*p::dsRed); *dre-1(ns39); nsIs25*

*nsEx3109 (aff-1*p::*dre-1*(654stop) cDNA + *unc-122*p::dsRed); *dre-1(ns39); nsIs25*

***dre-1* cDNA.** The new *dre-1* exon 1 was amplified from cDNA derived from mixed-stage *Caenorhabditis elegans* using primers ATGGCGGAGGAAGAAGAAGTGTCGAG-fwd and TGCTTCGGAGCTTCCCGATGGTG-rev to show that splicing over the 8.3-kb intron occurs. SL1 splicing was demonstrated using a forward primer corresponding to the SL1 sequence (GGTTTAATTACCCAAGTTTGAG-fwd) and a reverse primer within exon 1 (ATGGAAGAATGGTGACGAAGAGGACG-ACAT-rev).

***C. elegans* Germ-Line Transformation and Rescue.** All rescue experiments were performed using 5 ng/μL rescuing plasmid or fosmid + 15 ng/μL *unc-122*p::dsRed coinjection marker + 80 ng/μL pBluescript as carrier. Fluorescent reporters were injected at 25 ng/μL with the pRF4 *rol-6* plasmid as a coinjection marker (2).

RNA Interference. HT1114 *Escherichia coli* carrying the relevant RNAi plasmid from the Ahringer library (3) were grown overnight at 37 °C in LB + ampicillin. Bacteria were plated on NGM + isopropylthio-β-galactoside (1 mM) + carbenicillin (50 mg/mL) plates and incubated at 37 °C overnight. The following day, *rrf-3* (*pk1426*); *nsIs25* young adult hermaphrodites were placed on the lawn. For the next 2 d, L1 progeny were scored for tail-spike cell survival.

FBXO10 shRNAs were prepared in a doxycycline-inducible retroviral vector as described (4). shRNA sequences were as shown below.

S2 Cell Culture Studies. S2 cells were grown in Shields and Sang M3 insect medium with 10% (wt/vol) FBS and Penn-Strep at 50 units/mL at 25 °C. For transfections, 2 million cells in 2 mL of culture medium were placed into six-well plates, and the following day cells were transfected with ∼1 μg of plasmid DNA + 8 μL of Fugene HD Transfection Reagent (Roche). Analysis was performed 3 d later.

shFBXO10 #4	
bp1714-F	5′-GGCTGGCATTTACATCCTGTA
bp1714-R	5′-TACAGGATGTAAATGCCAGCC
shFBXO10 #5	
bp2433-F	5′-GGGGCAATGGTATCTATGACA
bp2433-R	5′-TGTCATAGATACCATTGCCCC
shFBXO10 #23	
bp828-F	5′-GTCACCCATCTGCAGATAAGA
bp828-R	5′-TCTTATCTGCAGATGGGTGAC

Plasmid Construction. For the *dre-1* transcriptional reporter, 4 kb of genomic DNA from the *dre-1* locus was amplified by PCR (GAAAGCGGCCGCCCGAGGGGACATC GAGATAGTA-fwd, CTTTACTAGTCTCCTGGCCAACCAGAGAC-rev) and the resulting amplicon was ligated into pPD95-69 at NotI/SpeI sites. For *dre-1* cDNA rescue constructs, the *dre-1* cDNA was amplified from purified mixed stage *C. elegans* cDNA and ligated via TOPO cloning into the pCRII-TOPO vector (Invitrogen). From this template, the *dre-1* cDNA was amplified (CTAGACTAGTATGGC-GGAGGAAGAA GAAGTGTCGAG and CTTTGTCGACTT-AAATTTCGGTGCCAGTCTCAGTGGA GATCG), and the resulting amplicon was ligated into pBluescript at SpeI/SalI sites. The *dre-1* 3′ UTR was amplified by PCR from genomic DNA (GTTTGTCGACCAACTGAGCG CCGGTCGCTAC-fwd, CTT-TGGGCCCGTACGGCCGACTAGTAGGAAACAGT-rev) and ligated with SalI and ApaI sites downstream of the *dre-1* cDNA in this plasmid. Finally, various promoters were amplified from genomic DNA and ligated using NotI and SpeI sites: 4.4 kb of genomic DNA upstream of the *aff-1* ATG was used for *aff-1*p::DRE-1 plasmids (CTAGGCGGCCGCCGGAAGGACGAGTAATACA-TGTTGCG-fwd, CTAGACTAGTCTGAAATTAAATAATTA-TAGGCTTTGAAATTGTGGG-rev); 730 bp of genomic DNA upstream of the *dpy-30* ATG was used for *dpy-30p*::DRE-1 plasmids (CTAGGCGGCCGCGTCTATTCTCACACCTCTCC-fwd, CTAGACTAGTTCTTGGTTTTTGCTCGATTT-rev).

For *Drosophila* S2 cell culture transfections, HA and myc tags were cloned into the pAC5.1 vector at KpnI/NotI sites using annealed oligos (CAAAATGTACCCATACGATGTTCCAGATT-ACGCTAAGCTTAGC-fwd, GGCCGCTAAGCTTAGCGTAA-TCTGGAACATCGTATGGGTACATTTTGGTAC-rev; CAA-AATGGAGCAGAAACTCATCTCTGAAGAGGATCTCAAG-CTTAGC-fwd, GGCCGCTAAGCTTGAGATCCTCTTCAGA-GATGAGTTTCTGCTCCATTTTGGTAC-rev). DRE-1, CED-9, and SKR-1 cDNAs were cloned downstream of these tags using NotI/ApaI sites (CTAGGCGGCCGCATGGCGGAGGAAGA-AGAAGTGTCGAG-fwd, CTAGGGGCCCTTAAATTTCGGT-GCCAGTCTCAGTGGAGATCG-rev; CTAGGCGGCCGCAT-GACACGCTGCACGGCGGAC-fwd, CGTAGGGCCCTTAC-TTCAAGCTGAACATCATCCGCC-rev; CTAGGCGGCCGC-ATGGCTGATCAAAAGAAAGTATCCGAGGCG-fwd, CTAG-GGGCCCTTAATCCTCGCACCAGGCATTCTCTTTGC-rev).

Flag-tagged FBXO10: FBXO10 cDNA clone (SC311108; Origene) was amplified with the primers (HindIII-Flag-FBOXO10-F: 5′-TCTATGTATAaagcttGCCACCATGG ACTACAAGGACG-ACGATGACAAGGAGGCTGGTGGCCTCCCCTTG; HindIII-FBXO10-R: 5′- TCTATGTATAaagcttTCACAGGATGGTGCA-GAAGACAC) and ligated into an inducible cytomegalovirus promoter/Tetracycline Operator (CMV/TO) retroviral vector with a selection marker puromycin, as described previously (4).

HA- or MYC-tagged BCL2: BCL2 cDNA (GC-B0284; Genecopoeia) was amplified with the primers HindIII-HA-BCL2-F

(5′-GCAATTGATCAAGCTTATGTA CCCATACGACGTC-CCAGACTACGCTATGGCGCACGCTGGGAGAAC); XhoI-BCL2-R (5′-GCAATTGATCCTCGAGTCACTTGTGGCTCA-GATAGGC) or primers BCL2-Hind-MYC-F (5′-GCAATTG-ATCAAGCTTATGGAACAAAAGCTGATCTCC GAAGAA-GACCTGATGGCGCACGCTGGGAGAAC) or XhoI-BCL2-R indicated above) and ligated into the same CMV/TO retroviral vector with a selection marker hygromycin, respectively.

Site-Directed Mutagenesis.

The following primers were used for the site-directed mutagenesis (200521-5; Stratagene) of FBXO10.

FBX10_R44H_F	CTCGACAGCACCCACTGGCGGCAGCTGTGTC
FBX10_R44H_R	GACACAGCTGCCGCCAGTGGGTGCTGTCGAG
FBX10_H212N_F	CAACTTTGAGAACGGGAACATCCAGGTCCATGG
FBX10_H212N_R	CCATGGACCTGGATGTTCCCGTTCTCAAAGTTG
FBX10_V762L_F	GGACAGAGGCATTACTTTGGCCCAGAGCAGCCAACCC
FBX10_V762L_R	GGGTTGGCTGCTCTGGGCCAAAGTAATGCCTCTGTCC
FBX10_R825W_F	CGATATCATTGGCAACTGGGGCAGCGGGCTGCAG
FBX10_R825W_R	CTGCAGCCCGCTGCCCCAGTTGCCAATGATATCG

Confocal Microscope Imaging. 293T cells were transduced with Flag-tagged FBXO10. Two days later, cells were transferred onto a coverslip inside a Petri dish filled with the DMEM growth medium for an additional day. Cells continued to grow at 37 °C in fresh growth medium with 250 nM of MitoTracker Red CMXRos (M7512; Invitrogen) for 45 min before fixation. Cells were fixed in 4% paraformaldehyde for 5 min, washed with 1× PBS three times, and then incubated with 0.5% Triton X-100 in 1× PBS for 5 min. After washing three times with 1× PBS, cells were incubated with Flag antibody (F3165; Sigma) for 1 h. Cells, washed once with 0.5% Triton X-100 in 1× PBS and three times with 1× PBS, were incubated with the secondary antibody anti-mouse Alexa Fluor 488 (Invitrogen) for 1 h. Cells were then washed once with 0.5% Triton X-100 in 1× PBS and three times with 1× PBS before imaging. Fluorescence images were acquired using a Zeiss LSM META laser scanning confocal microscope equipped with 63× plan-apochromat (N.A. 1.4) oil immersion objective lens (Carl Zeiss MicroImaging, Inc.).

Immunoprecipitation and Immunoblotting. Two to six milliliters of transfected S2 cells were pelleted by centrifugation and washed with 1 mL of cold PBS. Cells were lysed in 500 μL of lysis buffer [50 mM Tris·HCl (pH 7.5), 150 mM NaCl, 1% Nonidet P-40 (CA-630), and 2 mM EDTA] with protease inhibitor (11836153001; Roche) for 1 h at 4 °C. HA::DRE-1 was immunoprecipitated using anti-HA agarose beads (Genetex) for 3 h at 4 °C. Beads were washed three times with lysis buffer before denaturation. myc::CED-9 was immunoprecipitated with rabbit polyclonal anti-myc (ab9106; Abcam) + Protein A Dynabeads (Invitrogen) for 30 min at 20 °C. The complexes were isolated and washed with PBST according to the manufacturer's directions and denatured using lithium dodecyl sulfate (LDS) sample buffer (Invitrogen) at 95 °C for 5 min before analysis by SDS/PAGE on 4–12% *bis*-Tris gels (Invitrogen).

Ten to thirty million transfected 293T cells were washed once with cold PBS and lysed in 1× RIPA buffer [50 mM Tris·HCl (pH 8.0), 150 mM NaCl, 1.0% Nonidet P-40 (CA-630), 0.5% sodium deoxycholate, and 0.1% SDS] with proteinase inhibitor mixture (Sigma) and 1 mM PMSF (Sigma) for 1 h on ice. After centrifugation the supernatants were collected and incubated with the antibody in the cold room for 1 h with rotation before adding Protein A Agarose (20333; Pierce) or Protein G Agarose (20398; Pierce) for an additional 2 h. The agarose beads were washed with the buffer containing 50 mM Tris·HCl (pH 7.5), 150 mM NaCl, 1% Nonidet P-40 (CA-630), and 2 mM EDTA before denaturing the sample with LDS sample buffer (Invitrogen) at 100 °C for 5 min. Total proteins were separated on 4–12% SDS-polyacrylamide gels and transferred to nitrocellulose membranes.

The following antibodies were used for immunoprecipitation or immunoblotting: BCL2 (immunoprecipitation: 2870; Cell Signaling Technology; immunoblotting: sc-7382; Santa Cruz), MCL1 (sc-819; Santa Cruz), Flag (F3165; Sigma), β-actin (4967; Cell Signaling Technology), rat anti-HA peroxidase (3F10; Roche), CUL1 (sc-12761; Santa Cruz), biquitin (sc-8017; Santa Cruz), and rabbit anti-MYC (ab9106; Abcam).

In Vivo Ubiquitination Assay Under Denaturing Condition. 293T cells were cotransfected with HA-Ub (a gift from James Chen's laboratory, University of Texas Southwestern Medical Center, Dallas), Flag-FBXO10, and MYC-BCL2. Forty-eight hours later cells were treated with 250 nM PS-341 for an additional 4 h. The in vivo ubiquitination assay was performed under denaturing condition. Denatured cell extracts were prepared before immunoprecipitation by resuspending cell pellets in 100 μL of denaturing buffer [50 mM Tris (pH 7.5), 0.5 mM EDTA, 1% SDS, and 1 mM DTT]. Samples were boiled for 10 min and immunoprecipitations were carried out after addition of 900 μL of TNN buffer [50 mM Tris (pH 7.5), 0.25 M NaCL, 5 mM EDTA (pH 8.0), 0.5% Nonidet P-40, 50 mM NaF, 1 mM DTT, 1 mM PMSF, and 1× protease inhibitor mixture (P8340; Sigma)]. Immunoprecipitation complex with anti-MYC antibody was resolved by SDS/PAGE. The immunoblotting was performed with anti-HA peroxidase antibody.

Quantitative RT- PCR. Quantitative RT- PCR was performed using an ABI 7700 TaqMan machine for 40 cycles with annealing temperature of 60 °C using the following Applied Biosystems probes: FBXO10 (Hs00395472_m1), BCL2 (Hs00608023_m1), and β2 microglobulin (B2M) (Hs00187842_m1). Signal values were calculated using the ΔΔCt method (ABI), and gene expression was normalized to B2M.

FBXO10 Sequencing. Biopsy samples of various lymphoma patients for this study were described (5). The National Cancer Institute Institutional Review Board approved the study and written informed consent was obtained.

FBXO10 is screened by direct sequencing of PCR products generated from genomic DNA of patient samples. The following primers were designed to amplify all exons including the intron–exon boundaries. Primer pairs used to sequence exons of FBXO10 are listed in the table. Genomic DNA was amplified by PCR in a 20-μL reaction volume. Reactions contained 50–100 ng of genomic DNA, five picomoles each of forward and reverse primer, 250 μM each dNTP, 1× PCR buffer (GenScript) containing 100 mM Tris, 15 mM $MgCl_2$, 500 mM KCl, and 1.0 U of Taq polymerase. The thermal cycling conditions were as follows: 95 °C for 2 min, 35 cycles of 95 °C for 45 s, 60 °C for 45 s, 72 °C for 45 s, and the final extension at 72 °C for 10 min. Two microliters of the PCR products were analyzed by 2.0% agarose gel electrophoresis. Water (20 μL) was added to the remaining PCR product and purified with MinElute (Qiagene). Six microliters were then used in 10-μL sequencing reactions containing 3.2 pmol of primer, 1 μL of BigDye Terminator v1.1 ready reaction mix, and 2 μL of sequencing buffer (Applied Biosystems). Cycling conditions were 96 °C for 1 min and 35 cycles of 96 °C for 10 s, 55 °C for 10 s, and 60 °C for 4 min. DNA-sequencing reactions were purified with Performa@Ultra 96-Well Plate (Edge Bio). DNA-sequencing products were sequenced using ABI 3130 XL (Applied Biosystems) and analyzed with DNASTAR software.

Doxycycline-Inducible Cell Lines and Retroviral Transduction. All cell lines were cultured in Roswell Park Memorial Institute medium with 10–20% FBS. Engineered doxycycline-inducible cell lines expressing the bacterial tetracycline repressor were described

FBXO10 Exon 2_1 2F	GGGGACTGGTAAGTAGGATAGACAG
FBXO10 Exon 2_1 2R	CCCAACACTCAGGGTACGTC
FBXO10 Exon 2_2 3F	CAAGCAGCATTACCTTGCATC
FBXO10 Exon 2_2 3R	TCTGGGGTCAGAACTAGAAAGG
FBXO10 Exon 3_1 4F	AGGGCAGCTAGAGTCCAAAAC
FBXO10 Exon 3_1 4R	GTCTGGGCCACCCTTTCAC
FBXO10 Exon 3_2 5F	ACATTGTTATCGAGGGCAGC
FBXO10 Exon 3_2 5R	AAAATGCAAAATAGCCCCATC
FBXO10 Exon 4 6F	GACTCAGGTGTTCCTCCAGTG
FBXO10 Exon 4 6R	CGTAAATACAAGAGGGCAACG
FBXO10 Exon 5 7F	GCTGACGTGTCTGATCTGG
FBXO10 Exon 5 7R	AAATGGAGGAGAGACAGGGAG
FBXO10 Exon 6 8F	AAGAAGGCAGTCTCCTGGAAG
FBXO10 Exon 6 8R	GAGCAGTGTGAGGTCCTGAAG
FBXO10 Exon 7 9F	CCTATTTGCCAGCACTGGAG
FBXO10 Exon 7 9R	CCACAAGCTGGAGATGGAAC
FBXO10 Exon 8 10F	TCTCAGGGAGACTCAGGTGC
FBXO10 Exon 8 10R	AAAAGACAGTGGGGAGCC
FBXO10 Exon 9 11F	TTCCTGACTGGTGGTGTCAG
FBXO10 Exon 9 11R	AGGACTATCCCAGGGTTGTG
FBXO10 Exon 10 12F	CCCAGCTCTCCCACTCAG
FBXO10 Exon 10 12R	TTCAGGGAGCTTACTGTGGC
FBXO10 Exon 11 13F	GACTGTGCAGGGCATTCAG
FBXO10 Exon 11 13R	CAGGCAGTATTTCCACCTTAGC

previously (4). Doxycycline (20 ng/mL) was used for induction of gene expression.

A mixture of DNA constructs, the mutant ecotropic envelope-expressing plasmid pHIT/EA6 × 3*, and gag-pol–expressing plasmid pHIT60 was used to transfect the 293T cells using the Lipofectamine 2000 reagent (Invitrogen) as described previously (4). The retroviral supernatants were used to infect doxycycline-inducible lymphoma cells in the presence of 8 μg/mL polybrene in a single spin infection.

Apoptosis, Cell Cycle, and BCL2 Intracellular Flow Cytometric Analysis. Apoptosis was analyzed by FACS for intracellular cleaved polyADP ribose polymerase (PARP) and active caspase-3. Cells were fixed in PBS containing 2% paraformaldehyde and then permeabilized and costained with anti-PARP (clone F21-852; BD Pharmingen) and anti–caspase-3 (51-68655X; BD Pharmingen) antibodies diluted in FACS buffer (2% FBS in PBS) containing 0.25% saponin (Sigma).

Propidium iodide was used for a measurement of DNA content. Cells were fixed in cold 70% ethanol overnight and then washed and incubated with 1× PBS containing 40 μg/mL of propidium iodide (Sigma) and 100 μg/mL of RNase (Boehringer) for 30 min before FACS analysis.

PE mouse anti-human BCL2 antibody (556535; BD Pharmingen) was used for intracellular BCL2 measurement.

Isolation of Germinal Center B-Cell Populations. Human tonsils were obtained (with and in accordance with the Helsinski Protocols) as otherwise discarded "leftovers" from routine tonsillectomies at the Children's National Medical Center, Washington, DC. After mincing, tonsillar mononuclear cells were isolated by density centrifugation with Histopaque-1077 (Sigma). Naïve B cells and germinal center B cells were separated by magnetic cell separation with the MidiMACS system (Miltenyi Biotec) according to published protocols (6). The purity of the isolated primary B-cell subpopulations was determine by FACScan analysis (Becton Dickinson). Naïve B cells were IgD+ $CD38^{Low}$CD27– and germinal center B cells (centroblasts) were CD77+$CD38^{high}$.

Antibodies used for flow cytometry included fluorescein isothiocyanate-conjugated anti-IgD and anti-CD27, phycoeryhrin-conjugated anti-CD38 (BD Pharmingen) and anti-CD77 (Fisher), plus fluorescein isothiocyanate-conjugated anti-MURM (Immunotech). For detailed protocols see ref. 6.

1. Brenner S (1974) The genetics of Caenorhabditis elegans. *Genetics* 77(1):71–94.
2. Mello CC, Kramer JM, Stinchcomb D, Ambros V (1991) Efficient gene transfer in C.elegans: Extrachromosomal maintenance and integration of transforming sequences. *EMBO J* 10(12):3959–3970.
3. Kamath RS, Martinez-Campos M, Zipperlen P, Fraser AG, Ahringer J (2001) Effectiveness of specific RNA-mediated interference through ingested double-stranded RNA in Caenorhabditis elegans. *Genome Biol* 2(1):research 0002.1–0002.10.
4. Rui L, et al. (2010) Cooperative epigenetic modulation by cancer amplicon genes. *Cancer Cell* 18(6):590–605.
5. Lenz G, et al. (2008) Molecular subtypes of diffuse large B-cell lymphoma arise by distinct genetic pathways. *Proc Natl Acad Sci USA* 105(36):13520–13525.
6. Klein U, et al. (2003) Transcriptional analysis of the B cell germinal center reaction. *Proc Natl Acad Sci USA* 100(5):2639–2644.

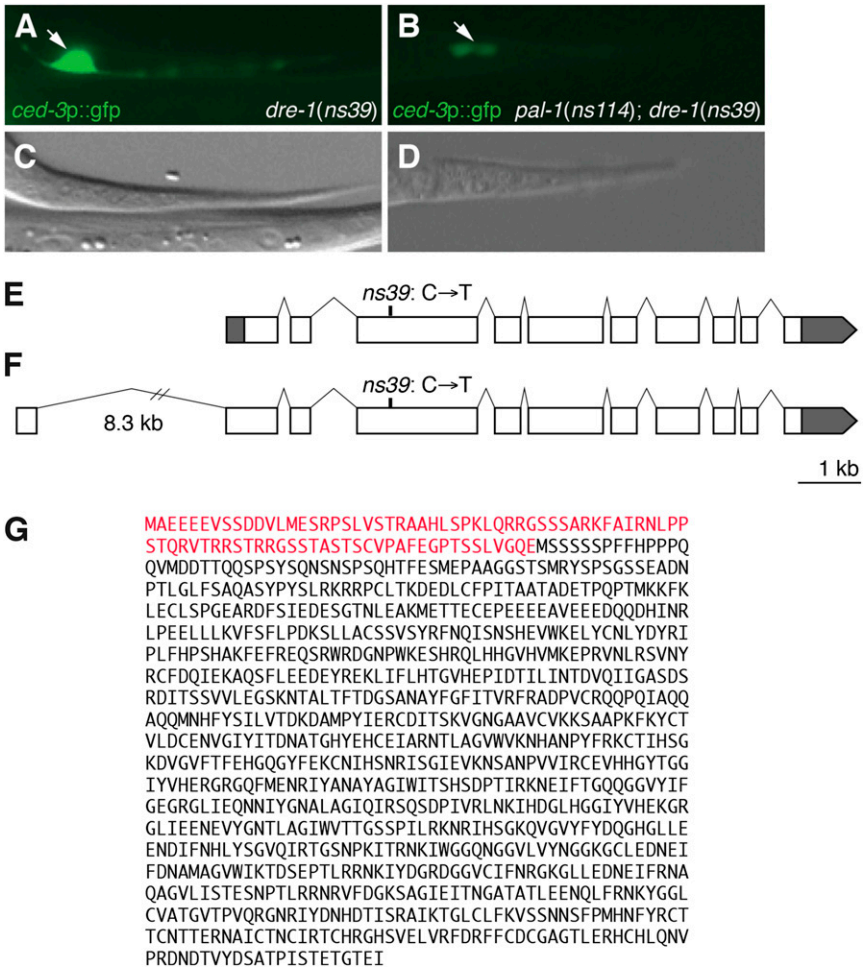

Fig. S1. *dre-1* does not regulate *ced-3* transcription. (*A* and *B*) Expression of a *ced-3*p::gfp reporter (*nsIs25*) in *dre-1*(*ns39*) (*A*) and *pal-1*(*ns114*); *dre-1*(*ns39*) (*B*) mutants. Arrow, position of the tail-spike cell body. (*C* and *D*) Differential interference contrast images of *A* and *B*, respectively. (*E* and *F*) Old (*E*) and new (*F*) predicted genomic structure of *dre-1*. Boxes, exons; lines, introns; white boxes, coding sequences; dark boxes, noncoding sequences. (*G*) DRE-1 protein sequence. Red, added new sequence.

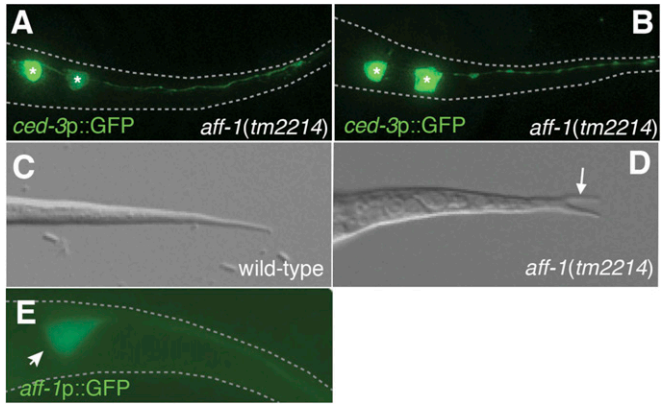

Fig. S2. *aff-1* is required for tail-spike cell fusion. (*A* and *B*) Fluorescence images of *aff-1*(*tm2214*) mutants expressing the *nsIs25* reporter transgene (*ced-3*p::GFP). Animals also contain the *ced-3*(*n717*) mutation. Asterisks, unfused tail-spike cell bodies. (*C* and *D*) Differential interference contrast images of tails of wild-type (*C*) or *aff-1*(*tm2214*) (*D*) L1 larvae. Arrow, forked tail. This is seen in 78% of *aff-1*(*tm2214*) L1s but not in *eff-1* mutants. (*E*) Fluorescence image of a wild-type animal expressing an *aff-1*p::GFP transgene. Arrow, tail-spike cell body.

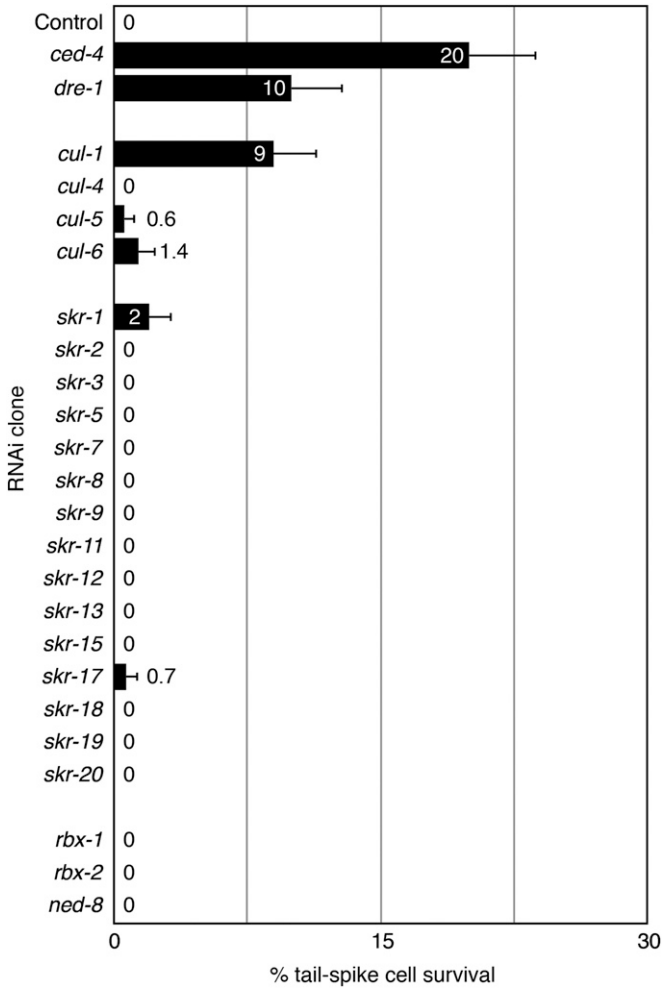

Fig. S3. Reverse genetic screen for SCF (Skp–Cullin–F-box) components with a role in tail-spike cell death. Histogram of results from a screen for SCF genes required for tail-spike cell death. Targeted animals had the *nsIs25* (*ced-3*p::gfp) transgene and the *rrf-3*(*pk1426*) RNAi sensitizing mutation. Numbers in bars, exact percentage of surviving cells; $n \geq 100$ for each RNAi clone. Error bar, SEM.

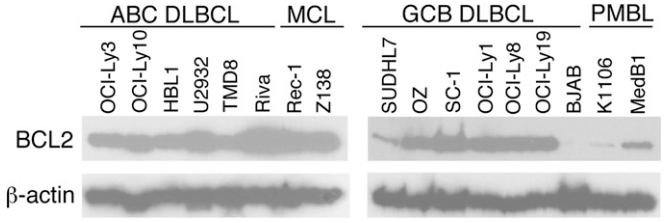

Fig. S4. BCL2 protein expression in lymphoma cell lines. MCL, mantle cell lymphoma; PMBL, primary mediastinal B-cell lymphoma.

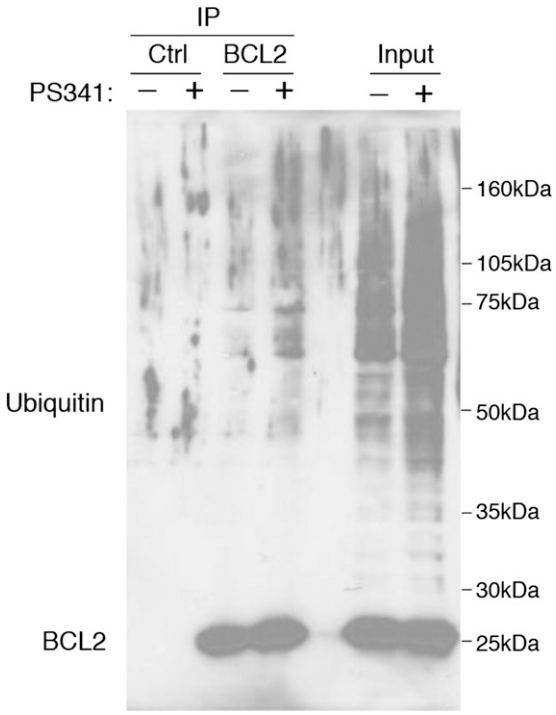

Fig. S5. BCL2 ubiquitination assay. HBL1 cells were treated with 250 nM PS-341 for 4 h before denaturation. Denatured cell extracts were prepared as in Fig. 3*F*. Samples were boiled for 10 min before immunoprecipitations with BCL2 antibody (2870; Cell Signaling Technology) or IgG control. The immunoblotting was performed with ubiquitin antibody (sc-8017; Santa Cruz) and BCL2 antibody (sc-7382; Santa Cruz).

Table S1. Screen for regulators of tail-spike cell death

Genotype[a]	% tail-spike cell survival[b]	No. extra cells[d]
Wild type	0 ± 0[c]	0 ± 0[e]
ns16	1 ± 1	0 ± 0
ns17	1 ± 1	0.1 ± 0.3
ns19	1 ± 1	0 ± 0
ced-3(*ns38*)	25 ± 4	7.2 ± 1
dre-1(*ns39*)	79 ± 3	0 ± 0
ns40	19 ± 4	0.1 ± 0.3
ns41	1 ± 1	0 ± 0
ced-3(*n2436*)	59 ± 8	4.2 ± 1.8
ced-3(*n2436*); *dre-1*(*ns39*)	100 ± 0	3.9 ± 1.6
Transgenic rescue of *dre-1*(*ns39*)		
dre-1(*ns39*); fosmid #1[f] line 1	2 ± 1	ND
dre-1(*ns39*); fosmid #2[g] line 1	7 ± 2	ND
dre-1(*ns39*); fosmid #2 line 2	13 ± 3	ND
dre-1(*ns39*); *dpy-30*p::*dre-1* cDNA line 1	30 ± 4	ND
dre-1(*ns39*); *dpy-30*p::*dre-1* cDNA line 2	46 ± 5	ND
dre-1(*ns39*); *aff-1*p::*dre-1* cDNA line 1	11 ± 3	ND
dre-1(*ns39*); *aff-1*p::*dre-1* cDNA line 2	22 ± 4	ND
dre-1(*ns39*); *aff-1*p::*dre-1* cDNA line 3	46 ± 5	ND

ND, not done.
[a]All strains contain the *nsIs23* or *nsIs25 C. briggsae ced-3*p::gfp integrated transgene to mark the tail-spike cell.
[b]n > 100 L1/L2 larvae scored for each genotype.
[c]Standard error of the mean.
[d]Average number of extra cells present in anterior pharynx.
[e]Mean ± standard deviation.
[f]WRM067bH07.
[g]WRM0637aG11.

Table S2. Effects of known *dre-1* interactors on tail-spike cell death

Genotype*	Tail-spike cell survival (%)†
Wild type	0 ± 0‡
dre-1(*ns39*)	79 ± 3
C05C8.6(*tm3719*)	1.5 ± 1
dre-1(*ns39*) *C05C8.6*(*tm3719*)	59 ± 3
gly-4(*ok2943*)	0.9 ± 0.9
gst-24(*ok3042*)	1.5 ± 1.2
Heterochronic mutants do not affect tail-spike cell death	
lin-29(*n333*)	0 ± 0
lin-28(*n719*)	0 ± 0
lin-46(*ma164*)	0.6 ± 0.3
lin-4(*e912*)	0.8 ± 0.8
daf-12(RNAi)	0 ± 0

*All strains contain the *nsIs25 Caenorhabditis briggsae ced-3*p::gfp integrated transgene to mark the tail-spike cell.
†$n > 100$ L1/L2 larvae scored for each genotype.
‡SEM.